

1 **European sulphate aerosols were a key driver of the early** 2 **twentieth-century intensification of the Asian summer monsoon**

3
4 Weihao Sun^{1,2}, Massimo A. Bollasina³, Ioana Colfescu^{4,5}, Guoxiong Wu⁶ and Yimin Liu⁶
5

6 ¹East China Sea Forecasting and Disaster Reduction Center, Ministry of Natural Resources, Shanghai, China

7 ²Observation and Research Station of Huaniaoshan East China Sea Ocean-Atmosphere Integrated Ecosystem,
8 Ministry of Natural Resources, Shanghai, China

9 ³School of GeoSciences, University of Edinburgh, Edinburgh, UK

10 ⁴School of Mathematics and Statistics, University of St Andrews, St Andrews, UK

11 ⁵National Centre for Atmospheric Science, UK

12 ⁶Key Laboratory of Earth System Numerical Modelling and Application, Institute of Atmospheric Physics,
13 Chinese Academy of Sciences, Beijing, China

14
15 Correspondence to: Massimo A. Bollasina (Massimo.Bollasina@ed.ac.uk)
16
17

18 **Abstract.** Observations show that the Asian summer monsoon experienced substantial multi-decadal changes
19 during the early 20th century, including a wetting trend over South Asia and a southward rainfall shift over East
20 Asia. Despite their significance, these variations have received limited attention, and the underlying mechanisms
21 remain poorly understood. This study investigates the role of increased European sulphate aerosol emissions in
22 shaping these monsoon changes using ensemble experiments with the Community Earth System Model. The
23 aerosol-driven rainfall patterns over South and East Asia resemble observations, suggesting that European
24 aerosols played an important role in modulating the monsoon. These changes are linked to large-scale anomalies
25 in surface climate and three-dimensional atmospheric circulation across the Indo-Pacific, which alter moisture
26 transport to the continent, the main driver of the rainfall anomalies. Regional circulation anomalies form part of a
27 hemispheric upper-tropospheric wave train originating over central Europe and extending through the Middle East
28 to the Pacific. The wave train arises as a thermodynamic adjustment to the aerosol-induced surface cooling and
29 related anticyclone over Europe, extends to the upper troposphere, and, while propagating eastward, induces three-
30 dimensional circulation anomalies across Asia that affect the monsoon. These findings provide compelling
31 evidence for the influence of European sulphate aerosols on the early 20th-century monsoon variability, which is
32 relevant for improving current understanding of the regional-scale impacts of anthropogenic aerosols. As
33 European SO₂ emissions continue to decline, this study sheds light upon a possible ongoing and future pathway
34 which may significantly modulate the monsoon response to Asian aerosol changes.

35 **1 Introduction**

36 The Asian summer monsoon (ASM) is a vital source of water for over 60% of the world's population (Turner and
37 Annamalai, 2012). Its interannual variability and long-term changes have significant implications for water
38 resources, agriculture, and economic activities across Asia (e.g., Gadgil and Rupa Kumar, 2006).

39
40 In the past decade, anthropogenic aerosols have attracted considerable scientific interest due to their ability to
41 offset part of the warming caused by greenhouse gases (GHGs) (e.g., Samset et al., 2018; Hegerl et al., 2019; Li
42 et al., 2022). Aerosols influence climate by scattering and absorbing solar radiation, and by acting as cloud
43 condensation and ice nuclei, thereby modifying cloud albedo, lifetime, and precipitation processes (Boucher et
44 al., 2013; Stier et al., 2024). They remain the largest source of uncertainty in estimating anthropogenic climate
45 forcing since the pre-industrial era (Andrews and Forster, 2020; Bellouin et al., 2020). While their global historical
46 effective radiative forcing is smaller than that of GHGs, aerosols can trigger strong regional climate responses due
47 to their spatial and temporal variability (e.g., Szopa et al., 2021).

48
49 The link between long-term changes in aerosol emissions and ASM variability is widely debated (e.g., Lau 2016;
50 Li et al., 2016; Wu et al., 2016). Research is particularly challenging due to the compounding effects of internal
51 variability, model biases, and divergent model responses (e.g., Saha and Gosh, 2019; Liu et al., 2024).
52 Nonetheless, studies using observational and modelling evidence have highlighted the significant impact of
53 aerosols, both regional (i.e., Asian-only) and remote (i.e., outside Asia), on the late 20th century weakening of the
54 South ASM and the emergence of a southern-flood-northern-drought (SFND) pattern over East Asia (e.g.,
55 Bollasina et al., 2011; Guo et al., 2013; Salzmänn et al., 2014; Li et al., 2015; Dong et al. 2019; Wilcox et al.
56 2020).

57
58 Gauge records reveal clear multi-decadal variability in both South Asian and East Asian summer monsoons
59 throughout the 20th century (e.g., Zhang and Zhou, 2011; Preethi et al., 2017; Li et al., 2023). In particular, the
60 first half of the century saw an increase in rainfall over South Asia, most notably in central India, and a tripole
61 pattern over East Asia, with excess rainfall in the south and northeast, and drier conditions along the Yangtze River
62 basin. These anomalies appear to be part of a coherent ASM-wide fluctuation, mirrored in broader Northern
63 Hemispheric summer monsoon changes (Zhang and Zhou, 2011; Preethi et al., 2017; Wang et al., 2018; Goswami

64 et al., 2023). Strikingly, this pattern reversed in the second half of the 20th century, producing comparable but
65 opposite sign anomalies, and resulting in minimal net change over the full period.

66

67 While monsoon changes since the 1950s have been extensively studied (e.g., Bollasina et al., 2011; Salzmann et
68 al., 2014; Song et al., 2014; Liu et al., 2019; Liu et al., 2024; Shao et al., 2024), early-century variations have
69 received less attention. Yet, given the contrasting trends throughout the historical period, understanding monsoon
70 drivers and the underpinning physical mechanisms in the entire record is essential to constrain the nature of its
71 multi-decadal variability and improve future projections. This is particularly relevant in the context of
72 disentangling internal climate variability from externally-forced changes (e.g., Salzmann and Cherian, 2015;
73 Huang et al., 2020). In this regard, compared to the later period, it is conceivable to assume a negligible role of
74 Asian aerosols in the first half of the 20th century, as emissions underwent a significant growth only from the
75 1950s and a sharp rise after the 1970s (Smith et al., 2011; Lund et al., 2019). In contrast, North American and
76 European aerosols had already increased substantially, raising the possibility of their significant influence on the
77 monsoon.

78

79 Several studies have highlighted the potential role of remote, including European, aerosols in driving Asian
80 summer monsoon changes (e.g., Cowan and Cai, 2011; Bollasina et al., 2014; Guo et al., 2015; Dong et al., 2016;
81 Liu et al., 2018; Shawki et al., 2018; Undorf et al., 2018a,b; Westervelt et al., 2018; Wang et al., 2020). However,
82 these analyses often relied on idealised simulations, such as long equilibrium experiments with present-day
83 emissions turned on or off. Whether aerosol influences were already detectable in the early 20th century remains
84 an open question. Addressing this gap is crucial for better understanding and narrowing uncertainty in aerosol-
85 related future monsoon projections, especially considering divergent present-day emission trends (e.g., Wang et
86 al., 2021a) and a wide range of plausible future pathways (Samset et al., 2019; Persad et al., 2023).

87

88 Against this backdrop, this study investigates whether rising European sulphate aerosols – the dominant
89 anthropogenic aerosol species of the region (e.g., Hoesly et al., 2018) – had any detectable impact on the ASM
90 during the first half of the 20th century. Section 2 introduces the climate model, experimental setup, and
91 observational data used. Section 3 presents the ASM response and examines the underlying mechanism.
92 Discussion and conclusions are provided in Section 4.

93 **2 Data and methods**

94 The primary data comprises output from two transient historical (1850–2005) experiments with the fully coupled
95 Community Earth System Model (CESM) version 1.2.2 (Hurrell et al., 2013). The atmospheric component is the
96 Community Atmospheric Model version 5.3 (CAM5.3, Neale et al., 2012), which includes a 3-mode aerosol
97 scheme and a prognostic representation of aerosol-cloud interactions (Ghan et al., 2012). The horizontal
98 resolutions are $1.9^\circ \times 2.5^\circ$ for the atmosphere and $0.6^\circ \times 0.9^\circ$ for the ocean. The model reproduces spatial patterns
99 and magnitude of the climatological summertime monsoon rainfall and low-tropospheric circulation reasonably
100 well (Supplementary Figure S1), consistent with the overall performance of CMIP5/CMIP6 models (Meehl et al.,
101 2020; He et al., 2023). A full description of the model and experiments is provided by Undorf et al. (2018a); here,
102 we briefly summarise key details.

103
104 Each experiment consists of an 8-member ensemble initialised from different points in a 200-year pre-industrial
105 (PI) simulation with fixed anthropogenic emissions at 1850 levels. The first experiment (ALL) includes time-
106 varying historical emissions of anthropogenic aerosols, greenhouse gases, and natural forcing factors. The second
107 (fixEU) is identical to ALL except that anthropogenic SO_2 and SO_4 emissions over Europe (EU) are held at PI
108 levels. Europe is defined according to Tier 1 regions from the Hemispheric Transport of Air Pollution 2
109 experiments (Koffi et al., 2016).

110
111 Several observational datasets are also used. Precipitation was taken from three land-only monthly gridded gauge-
112 based datasets to account for uncertainties and discrepancies: the $1^\circ \times 1^\circ$ Global Precipitation Climatology Centre
113 v2020 (GPCC; Schneider et al., 2014), the $0.5^\circ \times 0.5^\circ$ Climate Research Unit v4.00 (CRU; Harris et al., 2014),
114 and the $0.5^\circ \times 0.5^\circ$ University of Delaware v401 (UDEL, Willmott and Matsuura, 1995). Monthly sea level
115 pressure surface is from the $5^\circ \times 5^\circ$ Hadley Centre Sea Level Pressure dataset (HadSLP2; Allan and Ansell, 2006),
116 and 850-hPa winds from the ECMWF Reanalysis 5 (Hersbach et al., 2020). Monthly observed precipitation from
117 the $2.5^\circ \times 2.5^\circ$ Climate Prediction Center Merged Analysis of Precipitation dataset (CMAP, Xie and Arkin, 2017)
118 is also used for model validation.

119
120 The analysis focuses on the summer (June–August, JJA) monsoon variation during the early 20th century.
121 Temporal changes are estimated using least-squares linear trends from 1901 to 1955. Alternative trend estimation

122 methods (i.e., Sen's non-parametric slope or differences between the 1941–1955 and 1901–1915 means) yield
123 similar results (not shown). As the main objective is to isolate the influence of external forcing, particularly
124 anthropogenic aerosols, on the ASM, changes are primarily assessed using ensemble means. Assuming linear
125 additivity of responses, the difference between the ALL and fixEU experiments is interpreted as the impact of
126 European SO₂ emissions. Statistical significance is assessed using a two-tailed Student's *t*-test at the 90%
127 confidence level. To identify the contribution of the model's internal variability to the forced response, individual
128 ensemble members are also examined. Additionally, the PI simulation is used to assess the statistical significance
129 of the forced changes relative to internal variability. We generate 10,000 bootstrap samples of 8-member ensemble
130 means to construct the probability distribution of unforced linear trends; the 90% confidence interval is defined
131 as the range within which 90% of these fall.

132 **3 Results**

133 **3.1 Observed and simulated precipitation trends**

134 Observational data show that JJA precipitation changes across Asia during the first half of the twentieth century
135 exhibit a coherent large-scale pattern (Figure 1a), with robust features across multiple datasets (Supplementary
136 Figure S2). Over South Asia, significant wetting is observed across central and northern India, contrasted by
137 drying over southern and northeastern India, the eastern Himalayas and northern Myanmar. Further east, rainfall
138 deficits occur over southern Indochina and Indonesia, with a pronounced drying over the middle and lower reaches
139 of the Yangtze River valley (105°–120°E, 25°–35°N). In contrast, precipitation increases are seen in a band
140 extending from northern Indochina through southern China, and further north into northwestern China and the
141 Korean peninsula. Interestingly, the anomalous rainfall pattern over South Asia closely resembles, but with
142 opposite sign, that associated with the late 20th century weakening of the monsoon, while the anomalies over
143 eastern Asia are reminiscent of the reversed SFND pattern (e.g., BOLLASINA et al., 2011; DONG et al., 2016).

144

145 To provide further context on the long-term precipitation variations, Figure 1c shows the observed time series of
146 monsoon rainfall anomalies over the core Indian monsoon region (75°–87°E, 16°–27°N land-only points, see box
147 in Figure 1c). Beyond interannual and decadal fluctuations, the record reveals a marked increase from the 1900s
148 to the mid-1950s (+0.55/+0.76 mm day⁻¹ in GPCC/CRU over 55 years, statistically significant at the 90%
149 confidence level), equivalent to about 7–11% of the long-term climatology. The anomaly also results in a 5–7%

150 increase in the All-India rainfall relative to early-century values. A similar analysis over southern China (110°–
151 120°E, 25°–35°N; Supplementary Figure S3) also shows a prominent, statistically significant, multi-decadal trend.

152

153 Despite its coarser resolution, the ALL ensemble mean captures the main spatio-temporal characteristics of the
154 observed precipitation trends, although amounts are generally smaller (Figure 1b). The model reproduces the
155 observed widespread precipitation increase over northern India, albeit with a weaker magnitude ($+0.14 \text{ mm day}^{-1}$
156 $(55 \text{ years})^{-1}$ over the core region) and a slight eastward shift, and the drying over southern India. The model likely
157 underrepresents the full extent of the interaction with the Western Ghats. The simulated rainfall dipole over eastern
158 China aligns with observations, although the amounts are slightly underestimated. However, the model fails to
159 reproduce the observed wetting over southern China and northern Indochina, possibly due to limitations in
160 resolving interactions with the complex terrain. The sign of the core precipitation anomalies over India is
161 consistent across most of the individual ensemble members (6 out of 8), supporting a dominant anthropogenic
162 origin (Supplementary Figure S4).

163

164 Preventing European sulphate aerosols from increasing results in drier conditions over central-northern India and
165 the northern Bay of Bengal (BoB), with wetting over the eastern Himalayas and Myanmar. Concurrently, the
166 precipitation anomalies over eastern Asia reverse polarity, while a pronounced precipitation deficit appears over
167 Indochina. As a result, the precipitation pattern associated with increased European SO_2 emissions closely
168 resembles observations and shows greater similarity than ALL across Asia. The aerosol-related precipitation
169 response is also robust across most of the ensemble members (Supplementary Figure S4). For example, the
170 ensemble-mean rainfall trend over the core Indian region amounts to $+0.33 \text{ mm day}^{-1}$ over 55 years, with increases
171 in 6 out of 8 ensemble members. This indicates that European aerosols substantially contributed to the early 20th-
172 century ASM rainfall trends.

173

174 The observed and simulated 55-year rainfall trends over central-northern India are also compared with the
175 corresponding range of trends from the PI experiment (Supplementary Figure S4)). The trend from CRU is outside
176 the respective 90% confidence interval, while it is slightly below in GPCC. The trend from the ALL-ensemble
177 mean is within the corresponding 90% confidence interval ($+0.19 \text{ mm day}^{-1}$ over 55 years; Supplementary Figure
178 S5), although five of its members exhibit positive trends that are markedly discernible from internal variability.

179 The ensemble-mean drying trend in the fixEU experiment exceeds the 90% confidence level. As a result, the
180 ensemble-mean trend associated with European aerosols (EU) is clearly distinguishable from internally-generated
181 fluctuations, even exceeding the 95% confidence level (+0.24 mm day⁻¹ over 55 years).

182 **3.2 Changes in the monsoon circulation**

183 Changes in precipitation across Asia are closely linked with variations in near-surface and atmospheric circulation
184 patterns (Figure 2). The spatial correspondence between wet (dry) anomalies and regions of moisture flux
185 convergence (divergence) underscores the dominant role of circulation-induced moisture transport in shaping
186 monsoon precipitation trends (Figure 2b). Over South Asia, a prominent anomalous anticyclone centred over
187 southern India and the western BoB characterises the low-tropospheric flow. Over East Asia and the western
188 Pacific, a zonal dipole emerges: an anomalous cyclone spans northern Indochina, southeastern China, and the
189 South China Sea, accompanied by an elongated anticyclone extending from central China to the western Pacific.

190

191 As Figure 2a shows, strong low-level easterlies across southern India oppose the climatological westerlies from
192 the Arabian Sea, leading to local rainfall deficits. Meanwhile, the climatological moisture-laden southwesterlies
193 are deflected northward over the northern Arabian Sea. Upon reaching central and northern India, this flow
194 converges with anomalous northeasterlies from northern Indochina and the northern BoB, enhancing rainfall
195 (Figure 2b). On the western flank of the anomalous Indo-Pakistan low, dry northerlies suppress precipitation over
196 Pakistan. Over East Asia, enhanced Pacific moisture transport into southern China and northeastern Indochina,
197 opposing the climatological southerlies linked to the western Pacific subtropical high, leads to regional wetting.
198 Return westerlies south of the anomalous Pacific low further reinforce the moisture flux from the BoB,
199 contributing to widespread wetting across the Bay and northwestern Indochina. In contrast, reduced southerly
200 moisture advection brings drying to southern Indonesia and northeastern China.

201

202 Figure 2c shows that the regional upper-tropospheric circulation also exhibits substantial changes, consistent with
203 the tropical balance among convective heating, ascent, and upper-level divergence (and vice versa). Over northern
204 India and the northern BoB, strong mid-tropospheric ascent coincides with rainfall enhancement, accompanied by
205 divergent outflow in the upper troposphere. One branch heads northeastward, converging and subsiding over
206 Burma and central China. Other branches are directed southwestward and southward, with corresponding mid-
207 tropospheric subsidence and surface anticyclones over southern India and the northern equatorial Maritime

208 Continent. A meridional system of divergent cells over East Asia and the western Pacific reflects the deep
209 convection and upper-tropospheric divergence centred near 20°N. The southern cell also converges and subsides
210 over the north equatorial Maritime Continent, aligning with the southern outflow from South Asia.

211 **3.3 Aerosol forcing over Europe**

212 To elucidate the generating mechanism, Figure 3a shows the widespread sulphate loading anomaly over Europe
213 resulting from enhanced emissions. Once emitted, aerosols are transported across and beyond the Continent.
214 Notably, aerosols spread southwestward towards northern Africa and the tropical Atlantic via the summertime
215 climatological circulation of the Azores high, and eastward over central Eurasia by the midlatitude climatological
216 westerlies, displacing the maximum loading and Aerosol Optical Depth (AOD; Supplementary Figure S6)
217 eastward of the emissions source.

218

219 Consistent with this transport, surface clear-sky downward shortwave radiation decreases across Europe, with
220 anomalies exceeding -3 W m^{-2} over 55 years in regions of peak aerosol loading (Figure 3b), accounting for
221 approximately 80% of the local reduction in the all-sky radiation (Supplementary Figure S6). All-sky radiation
222 anomalies are larger (up to -5 W m^{-2}) due to increased cloudiness associated with circulation changes (see last
223 paragraph in this Section). As expected by the aerosol scattering effect, net shortwave differences between the
224 top-of-atmosphere and surface are minimal (Supplementary Figure S6). Including longwave effects, the net
225 radiative cooling at the model top reached about -2 W m^{-2} over central and eastern Europe (Supplementary Figure
226 S6).

227

228 Cloud droplet number concentration displays widespread positive anomalies over central and eastern Europe
229 concurrently with a negative, albeit weak, decrease in cloud top effective radius (Supplementary Figure S6). These
230 changes are consistent with those expected by the cloud response to sulphate aerosols, assuming negligible
231 variations in water liquid content. The latter remains relatively unchanged or slightly enhanced due to anomalous
232 northwesterlies from the Atlantic (see next paragraph).

233

234 As a result of the aerosol-induced dimming, near-surface temperature shows anomalous cooling over central and
235 eastern Europe (Figure 3c), and concurrently, the circulation adjusts thermodynamically, with marked anticyclonic
236 anomalies occurring at the surface. Interestingly, Figure 3d shows that the largest cooling and the high-pressure

237 core are displaced east of the aerosol loading maximum, suggesting the combined influence of direct forcing,
238 feedbacks, and modulation by the climatological flow. For example, eastward aerosol transport and temperature
239 advection by the climatological westerlies contribute in concert to displacing the aerosol cooling to the east. The
240 associated northeasterly flow on the eastern flank of the surface anticyclone further reinforces the cooling over
241 eastern Europe. Note that the simulated northeastward displacement of the anomalous anticyclone is consistent
242 with the displacement shown by observed sea-level pressure trends (Supplementary Figure S7).

243 **3.4 Rossby wave propagation and remote teleconnections**

244 As shown in Figure 4, the regional signature of European aerosols extends to the mid and upper troposphere.
245 Streamfunction anomalies feature a (weak) equivalent-barotropic nature and a slight northwestward tilt with
246 height (not shown), consistent with the mature phase of an extratropical disturbance. At 300 hPa, anticyclonic
247 anomalies are seen over central Europe. This pattern forms part of a wave train signal extending across the
248 northern hemisphere, indicating a Rossby wave response to increased European aerosols and related upper-level
249 relative vorticity anomalies, which serve as the primary source of wave activity.

250

251 Upper-level meridional wind anomalies align with expectations from the streamfunction/geopotential height
252 pattern, revealing alternating cyclonic and anticyclonic centres (Figure 4b). The wave activity flux (e.g., Takaya
253 and Nakamura 2001) highlights two eastward propagation branches. The main branch extends southeastward
254 across the Middle East to Pakistan and northwestern India, where it weakens while turning northeastward into
255 eastern China and converges over Japan. This flux follows the Asian jet stream, which acts as a Rossby waveguide.

256 A secondary, weaker high-latitude pathway is also evident: the wave flux points northeastward towards northern
257 Russia, crosses northern Eurasia, and then turns southeastward over the northwestern Pacific, ultimately
258 converging with the main pathway.

259

260 Mid-tropospheric ascent and descent anomalies accompany the wave train (Figure 4b), consistent with the
261 vorticity balance (e.g., Rodwell and Hoskins 2001). For example, the anticyclonic anomaly over Afghanistan and
262 Pakistan induces southward flow and subsidence to its east, suppressing precipitation over Pakistan and the
263 western Tibetan Plateau. Conversely, an anomalous upper-tropospheric anticyclone develops over eastern China
264 and the western Pacific (120°-140°E). Northward flow and ascent occur on its western flank, while subsidence is
265 found to the east, in agreement with the fundamental vorticity balance. At lower levels, this configuration

266 generates an anomalous westerly flow from the western Pacific toward south-eastern China, enhancing moisture
267 transport and producing a positive precipitation anomaly. This rainfall anomaly, in turn, drives strong variations
268 in the tropical divergent circulation: part of the divergent outflow extends toward the Maritime Continent, where
269 it converges, descends, and produces anomalous anticyclonic flow. The interaction between extratropical wave-
270 induced anomalies over eastern China/western Pacific and the resulting meridional adjustments in the tropical
271 divergent circulation account for the characteristic tripolar anomalous rainfall pattern across East Asia. These
272 results suggest that key upper-tropospheric action centres, over the Middle East and southern China/western
273 Pacific, initiate low-tropospheric circulation adjustments that generate the anomalous rainfall pattern across Asia.

274 **4 Discussion and concluding remarks**

275 The Asian summer monsoon hydroclimate underwent significant changes in the early 20th century, characterised
276 by a wetting trend over South Asia and a southern rainfall shift over East Asia. This study finds that increased
277 European anthropogenic sulphate aerosols played a key role in driving these observed monsoon changes. The
278 aerosol-induced cooling and large-scale anticyclonic anomaly over central/eastern Europe extend from the surface
279 to the upper troposphere. These anomalies trigger subsequent atmospheric circulation adjustments in the form of
280 an eastward propagating Rossby-wave train, which is central to realising the remote aerosol impact across Asia.

281

282 These findings shed new light on the drivers and mechanisms of monsoon multidecadal variability. While most
283 existing research has focused on recent monsoon changes, the early historical period remains unexplored.
284 Moreover, many prior studies have relied on long, equilibrium-type experiments to enhance the signal-to-noise
285 ratio, but these are less representative of the transient response to evolving aerosol emissions. An atmospheric
286 propagation pathway similar to the one identified here has been discussed in earlier literature, particularly in
287 relation to the downstream signature of the North Atlantic Oscillation (e.g., Watanabe 2004) and broader
288 teleconnections between Europe and East Asia (e.g., Lu et al. 2002; Enomoto et al., 2003), yet it has been largely
289 overlooked in the context of aerosol forcing (e.g., Wang et al., 2021b), which has instead typically emphasised
290 changes in the large-scale meridional temperature gradient across Eurasia as the dominant key mechanism.

291

292 Placing our study within the broader literature on remote aerosol-monsoon interactions underscores its relevance.
293 Cowan and Cai (2011) were among the first to identify the influence of non-Asian aerosols, primarily European

294 sulphate, in weakening the ASM over the 20th century by inducing widespread Eurasian cooling and thereby
295 reducing the meridional temperature gradient, which in turn weakens the southerly monsoon flow. Similarly, Guo
296 et al. (2015, 2016) linked widespread drying across Asia to increased global aerosol emissions, mainly from non-
297 Asian sources, and the subsequent modulation of the zonal-mean meridional temperature gradient. Focusing on
298 the fast, atmospheric-only equilibrium response to the removal of European aerosols, Dong et al. (2016) reported
299 a strengthening of the South Asian monsoon and a southern shift in East Asian rainfall, attributed to the
300 downstream advection of cooler, drier air from Europe to Asia and consequent weakening of the tropospheric
301 thermal gradient. Shawki et al. (2018) similarly found that removing European aerosol emissions strengthens,
302 albeit weakly, the South Asian monsoon and shifts the East Asian monsoon northward, via changes in the large-
303 scale temperature gradient and the interhemispheric heat and moisture transport. Liu et al. (2018) reported a slight
304 decrease in annual mean precipitation over Asia associated with increased European sulphate aerosols, driven by
305 the slow (ocean-mediated) component of the total response via inter-hemispheric heating redistribution. Similar
306 rainfall patterns were also shown by Westervelt et al. (2018). More recently, Wang et al. (2017) and Wang et al.
307 (2020) highlighted that non-local aerosol emissions are as influential as local ones in weakening the East Asian
308 summer monsoon, primarily through easterly advection of colder air across Eurasia and resulting change in
309 meridional heat transport, in agreement with Dong et al. (2016).

310

311 An enhanced meridional temperature gradient between central Eurasia and the IO is a well-known contributor to
312 stronger monsoon precipitation over South Asia (e.g., Meehl and Arblaster, 2002). Indeed, this has been identified,
313 for example, as one of the elements contributing to enhanced future monsoon precipitation by the end of the 21st
314 century (e.g., Meehl et al., 2024). This outcome, however, is not borne out in our study, as the mid and high
315 troposphere temperature averaged over the 60°-100°E sector displays enhanced cooling compared to the north-
316 equatorial IO, resulting in a weaker meridional temperature gradient (not shown). This discrepancy indicates that
317 the aerosol-induced regional monsoon circulation and precipitation variations over South Asia cannot be explained
318 by broad-scale sector-mean temperature changes. On the contrary, the anomalous temperature pattern over Eurasia
319 displays a close relationship with that induced by the anomalies in atmospheric advection, especially in the
320 meridional direction, in turn associated with the upper-tropospheric wave train.

321

322 This dynamical pathway and the critical role of large-scale remotely driven atmospheric dynamical changes finds

323 support in Bollasina et al. (2014). Although secondary to regional emissions in explaining the recent monsoon
324 rainfall decline, extratropical aerosols were nonetheless shown to induce widespread temperature and wind
325 anomalies across Asia, revealing the complex interplay between aerosol forcing, precipitation, and circulation
326 changes. Undorf et al. (2018a, b) also highlighted the importance of midlatitude aerosol forcing in explaining the
327 observed weakening of the South Asian monsoon through the mid-1970s, underscoring the key role of Eurasian-
328 scale dynamical adjustments.

329

330 An important question is whether Indian Ocean (IO) SSTs also influenced the monsoon. The ALL ensemble,
331 consistent with the overall performance of CMIP5/6 models (e.g., Roxy et al., 2014), exhibits widespread and
332 relatively homogeneous warming across the basin. In contrast, aerosol-induced SST trends, albeit weak, show
333 warming over the western equatorial IO and cooling over the subequatorial regions (Supplementary Figure S8).
334 This cross-equatorial dipole in SST trends is also evident, and more pronounced, in observations (e.g., Figure 3
335 in Goswami et al., 2023), which suggests an aerosol contribution to the IO warming pattern. Further analysis of
336 the EU ensemble (Supplementary Figure S8), shows that SST anomalies are largely anticorrelated with
337 evaporation: reduced evaporation dominates the western and equatorial IO, while increases are seen in the south.
338 Concurrently, anomalous near-surface divergent easterlies across the north-equatorial IO oppose the
339 climatological (south) westerlies, reducing evaporation and upwelling, which contribute to warming the SSTs.
340 These patterns are similar to those associated with the Indian summer monsoon multi-decadal variability during
341 the 20th century (Goswami et al., 2023). Also, the 55-year SST pattern resembles 20th-century-long changes,
342 although the latter exhibits weaker anomalies and a less pronounced cooling (e.g., Rao et al., 2012; Roxy et al.,
343 2014). Uncertainties remain in identifying the causes of the persistent western IO warming due to strong feedbacks
344 between oceanic anomalies, atmospheric circulation, and convection (e.g., Rao et al., 2012; Swapna et al., 2014).
345 While our findings highlight the role of remotely-forced wind anomalies, other mechanisms may also contribute.
346 While SST anomalies and rainfall are anticorrelated in the long term, this relationship reverses in the early 20th
347 century (Figure 3 in Roxy et al., 2015), aligning with our findings.

348

349 Our results have important implications. They suggest that non-local anthropogenic aerosols have contributed
350 significantly to shaping monsoon variability even during the early historical period. This is particularly relevant
351 for understanding regional-scale impacts of anthropogenic forcing, which remain uncertain due to the spatial

352 heterogeneity of emissions and their diverse climate effects. Importantly, under the current continued decrease in
353 European aerosol emissions, assuming an opposite ASM response to the one described above, remotely-driven
354 precipitation anomalies may significantly modulate, if not partially offset, the response to Asian aerosol emission
355 changes (already declining or expected to do so in the future; e.g., Lund et al., 2019; Xiang et al. 2023). For
356 example, assuming linearity in the combined responses, the abatement of EU sulphate aerosols would lead to a
357 weaker monsoon over most of South Asia, and India in particular, which is opposite to the expected wetting
358 associated with decreased sulphate aerosols over both South and East Asia (e.g., Bartlett et al., 2018). Conversely,
359 EU aerosol reductions would contribute to further amplify the reversed SFND pattern over China brought about
360 by decreased East Asian aerosol alone (e.g., Dong et al., 2016), resulting, for example, in enhanced drying over
361 southeastern China. While the future monsoon response to the projected decline in worldwide aerosol emissions
362 will most likely result from non-linear interactions among the different aerosol source regions, the above picture
363 illustrates the complex interplay among local and remote aerosols and the need for a consistent and coordinated
364 modelling and analysis approach (e.g., Wilcox et al., 2023).

365

366 While our analysis emphasises the central role of European aerosols, other remote emissions (e.g., from North
367 America) and external forcings (e.g., greenhouse gases) may have also played a role. Our conclusions are based
368 on ensemble experiments comprising eight members each, consistent with the minimum number typically
369 recommended for detecting forced multi-decadal signals (e.g., Deser et al., 2012). However, internal variability
370 cannot be ruled out, and studies have, for example, discussed the association of Atlantic slow-frequency variability
371 with the ISM multi-decadal mode (e.g., Rajesh and Goswami, 2020). In this context, the use of large single-forcing
372 ensembles (e.g., Smith et al., 2022; Simpson et al., 2023) offers a promising approach to disentangling the
373 individual contributions of greenhouse gases, anthropogenic aerosols and other external drivers. Furthermore, our
374 findings are based on a single climate model and therefore depend on its representation of aerosol-cloud-radiation
375 and circulation interactions. Given the well-known uncertainties in aerosol forcing and its climatic effects, the
376 response may differ across models and from real-world observations. For example, CESM1 is known to exhibit a
377 relatively strong aerosol effective radiative forcing (Zelinka et al., 2014; 2023), which may result in a stronger
378 climate response to aerosol perturbations than seen in other models.

379

380 **Acknowledgements.** MAB acknowledges support from the Natural Environment Research Council
381 (NE/N006038/1) and the Research Council of Norway (grant no. 324182; CATHY).

382

383 **Data availability.** GPCC data are retrieved from <https://psl.noaa.gov/data/gridded/data.gpcc.html>, CRU data from
384 <https://crudata.uea.ac.uk/cru/data/hrg/>, and UDEL data from
385 https://psl.noaa.gov/data/gridded/data.UDe1_AirT_Precip.html. The ERA5 data are obtained at
386 <https://cds.climate.copernicus.eu/datasets/reanalysis-era5-pressure-levels-monthly-means>. HadISST data are
387 available from <https://www.metoffice.gov.uk/hadobs/hadisst/>, while the HadSLP2 dataset is accessed from
388 <https://www.metoffice.gov.uk/hadobs/hadslp2/>. The CESM model data used in this study are available from MAB
389 upon request.

390

391 **Author contribution.** WS and MAB designed the study. WS performed the analysis and completed the first draft
392 of the manuscript. WS and MAB discussed the results, WA, MAB, and IC edited the manuscript. GW and YL
393 provided suggestions on the analysis and interpretation of the results.

394

395 **Competing interests.** The authors have no competing interests to declare.

396

397 **References**

- 398 Allan, R., and Ansell, T.: A New Globally Complete Monthly Historical Gridded Mean Sea Level Pressure Dataset
399 (HadSLP2): 1850–2004, *J. Climate*, 19, <https://doi.org/10.1175/JCLI3937.1>, 2006.
- 400 Andrews, T., and Forster, P.M.: Energy budget constraints on historical radiative forcing, *Nat. Clim. Chang.* 10,
401 <https://doi.org/10.1038/s41558-020-0696-1>, 2020.
- 402 Bartlett, R. E., Bollasina, M. A., Booth, B. B. B. et al.: Do differences in future sulfate emission pathways matter
403 for near-term climate? A case study for the Asian monsoon, *Clim. Dynam.*, 50, [https://doi.org/10.1007/s00382-](https://doi.org/10.1007/s00382-017-3726-6)
404 [017-3726-6](https://doi.org/10.1007/s00382-017-3726-6), 2018.
- 405 Bellouin, N., et al.: Bounding aerosol radiative forcing of climate change, *Rev. Geophys.*, 58,
406 <https://doi.org/10.1029/2019RG000660>, 2020.
- 407 Bollasina, M.A, Ming, Y, Ramaswamy, V.: Anthropogenic aerosols and the weakening of the South Asian summer
408 monsoon, *Science*, 334, <https://doi.org/10.1126/science.1204994>, 2011.
- 409 Bollasina, M. A., Ming, Y., Ramaswamy, V., Schwarzkopf, M. D., and Naik, V.: Contribution of local and remote
410 anthropogenic aerosols to the twentieth century weakening of the South Asian monsoon, *Geophys. Res. Lett.*,
411 41, <https://doi.org/10.1002/2013GL058183>, 2014.
- 412 Boucher, O., Randall, D., Artaxo, P., Bretherton, C., Feingold, G., Forster, P., Kerminen, V.-M., Kondo, Y., Liao,
413 H., Lohmann, U., Rasch, P., Satheesh, S., Sherwood, S., Stevens, B., and Zhang, X.: Clouds and aerosols, in
414 *Climate change 2013: The physical science basis. Contribution of Working Group I to the Fifth Assessment*
415 *Report of the Intergovernmental Panel on Climate Change*, edited by Stocker T., Qin D., Plattner G.-K., Tignor
416 M., Allen S., Boschung J., Nauels A., Xia Y., Bex V., and Midgley P., chap. 7, pp. 571–658, Cambridge
417 University Press, Cambridge, United Kingdom and New York, NY, USA,
418 <https://10.1017/CBO9781107415324.016>, 2013.
- 419 Cowan, T. and Cai, W.: The impact of Asian and non-Asian anthropogenic aerosols on 20th century Asian summer
420 monsoon, *Geophys. Res. Lett.*, 38, <https://doi.org/10.1029/2011GL047268>, 2011.
- 421 Deser, C., Phillips, A., Bourdette, V., et al.: Uncertainty in climate change projections: the role of internal
422 variability, *Clim. Dynam.*, 38, <https://doi.org/10.1007/s00382-010-0977-x>, 2012.
- 423 Dong, B., Sutton, R. T., Highwood, E. J., and Wilcox, L. J.: Preferred response of the East Asian summer monsoon
424 to local and non-local anthropogenic sulphur dioxide emissions, *Clim. Dynam.*, 46,
425 <https://doi.org/10.1007/s00382-015-2671-5>, 2016.

426 Dong, B., Wilcox, L.J., Highwood, E.J., and Sutton, R. T.: Impacts of recent decadal changes in Asian aerosols on
427 the East Asian summer monsoon: roles of aerosol–radiation and aerosol–cloud interactions, *Clim. Dynam.*,
428 53, <https://doi.org/10.1007/s00382-019-04698-0>, 2019.

429 Enomoto, T., Hoskins, B.J., and Matsuda, Y.: The formation mechanism of the Bonin high in August, *Q. J. Roy.*
430 *Meteor. Soc.*, 129, <https://doi.org/10.1256/qj.01.211>, 2003.

431 Gadgil, S., and Rupa Kumar, K.: The Asian monsoon — agriculture and economy. In: *The Asian Monsoon*.
432 Springer Praxis Books. Springer, Berlin, Heidelberg. https://doi.org/10.1007/3-540-37722-0_18, 2006.

433 Ghan, S. J., Liu, X., Easter, R. C., Zaveri, R., Rasch, P. J., et al.: Toward a minimal representation of aerosols in
434 climate models: Comparative decomposition of aerosol direct, semidirect, and indirect radiative forcing, *J.*
435 *Climate*, 25, <https://doi.org/10.1175/JCLI-D-11-00650.1>, 2012.

436 Goswami, D. J., Ashok, K., and Goswami, B. N.: Local ocean–atmosphere interaction in Indian summer monsoon
437 multi-decadal variability, *Clim. Dynam.*, 60, <https://doi.org/10.1007/s00382-022-06377-z>, 2023.

438 Guo, L., Highwood, E. J., Shaffrey, L. C., and Turner, A. G.: The effect of regional changes in anthropogenic
439 aerosols on rainfall of the East Asian summer monsoon, *Atmos. Chem. Phys.*, 13, [https://doi.org/10.5194/acp-](https://doi.org/10.5194/acp-13-1521-2013)
440 [13-1521-2013](https://doi.org/10.5194/acp-13-1521-2013), 2013.

441 Guo, L., Turner, A. G., and Highwood, E. J.: Impacts of 20th century aerosol emissions on the South Asian
442 monsoon in the CMIP5 models, *Atmos. Chem. Phys.*, 15, <https://doi.org/10.5194/acp-15-6367-2015>, 2015.

443 Harris, I., Jones, P.D., Osborn, T.J. and Lister, D.H.: Updated high-resolution grids of monthly climatic
444 observations – the CRU TS3.10 Dataset, *Int. J. Climatol.*, 34, <https://doi.org/10.1002/joc.3711>, 2014.

445 He, L., Zhou, T., and Chen, X.: South Asian summer rainfall from CMIP3 to CMIP6 models: biases and
446 improvements, *Clim. Dynam.*, 61, <https://doi.org/10.1007/s00382-022-06542-4>, 2023.

447 Hegerl G.C., Bronnimann S., et al.: Causes of climate change over the historical record, *Environ. Res. Lett.*, 14,
448 <https://doi.org/10.1088/1748-9326/ab4557>, 2019.

449 Hersbach, H., Bell, B., Berrisford, P., et al.: The ERA5 global reanalysis. *Q. J. Roy. Meteor. Soc.*, 146,
450 <https://doi.org/10.1002/qj.3803>, 2020.

451 Hoesly, R.M., et al.: Historical (1750–2014) anthropogenic emissions of reactive gases and aerosols from the
452 Community Emissions Data System (CEDS), *Geosci. Model Dev.*, 11, [https://doi.org/10.5194/gmd-11-369-](https://doi.org/10.5194/gmd-11-369-2018)
453 [2018](https://doi.org/10.5194/gmd-11-369-2018), 2018.

454 Huang, X., and Coauthors: The recent decline and recovery of Indian summer monsoon rainfall: relative roles of

455 external forcing and internal variability, *J. Climate*, 33, <https://doi.org/10.1175/JCLI-D-19-0833.1>, 2020.

456 Hurrell, J. W., Holland, M. M., Gent, P. R., Ghan, S., Kay, J. E., et al.: The Community Earth System Model, *Bull.*
457 *Amer. Met. Soc.*, 94, <https://doi.org/10.1175/BAMS-D-12-00121.1>, 2013.

458 Koffi, B., Dentener, F., Janssens-Maenhout, G., Guizzardi, D., Crippa, M., et al.: Hemispheric transport air
459 pollution (HTAP): Specification of the HTAP2 experiments ensuring harmonized modelling (Tech. rep.)
460 Luxembourg: Joint Research Centre JRC. <https://doi.org/10.2788/725244>, 2016.

461 Lau, W.K.M.: The aerosol-monsoon climate system of Asia: A new paradigm, *J. Meteor. Res.*, 30,
462 <https://doi.org/10.1007/s13351-015-5999-1>, 2016.

463 Li, X., Li, Q., Ding, Y., Yang, S., et al.: Possible influence of the interdecadal variation of the extratropical southern
464 Indian Ocean SST on East Asian summer monsoon precipitation, *Atmos. Res.*, 288,
465 <https://doi.org/10.1016/j.atmosres.2023.106721>, 2023.

466 Li, X., Ting, M., Li, C., and Henderson, N.: Mechanisms of Asian summer monsoon changes in response to
467 anthropogenic forcing in CMIP5 models, *J. Climate*, 28, <https://doi.org/10.1175/JCLI-D-14-00559.1>, 2015.

468 Li, Z., et al.: Aerosol and monsoon climate interactions over Asia, *Rev. Geophys.*, 54,
469 <https://doi.org/10.1002/2015RG000500>, 2016.

470 Li, J., Carlson, B.E., Yung, Y.L., et al.: Scattering and absorbing aerosols in the climate system, *Nat. Rev. Earth*
471 *Environ.*, 3, <https://doi.org/10.1038/s43017-022-00296-7>, 2022.

472 Liu, L., Shawki, D., Voulgarakis, A., Kasoar, M., Samset, B. H., et al.: A PDRMIP Multimodel study on the
473 impacts of regional aerosol forcings on global and regional precipitation, *J. Climate*, 31,
474 <https://doi.org/10.1175/JCLI-D-17-0439.1>, 2018.

475 Liu, Y., Cai, W., Sun, C., Song, H., Cobb, K. M., et al.: Anthropogenic aerosols cause recent pronounced
476 weakening of Asian summer monsoon relative to last four centuries, *Geophys. Res. Lett.*, 46, 5469–5479,
477 <https://doi.org/10.1029/2019GL082497>, 2019.

478 Liu, Z., Bollasina, M. A., and Wilcox, L. J.: Impact of Asian aerosols on the summer monsoon strongly modulated
479 by regional precipitation biases, *Atmos. Chem. Phys.*, 24, 7227–7252, [https://doi.org/10.5194/acp-24-7227-](https://doi.org/10.5194/acp-24-7227-2024)
480 [2024](https://doi.org/10.5194/acp-24-7227-2024), 2024.

481 Lu, R.-Y., Oh, J.H., and Kim, B.J.: A teleconnection pattern in upper-level meridional wind over the North African
482 and Eurasian continent in summer, *Tellus A*, 54, <https://doi.org/10.3402/tellusa.v54i1.12122>, 2002.

483 Lund, M. T., Myhre, G., and Samset, B. H.: Anthropogenic aerosol forcing under the Shared Socioeconomic

484 Pathways, Atmos. Chem. Phys., 19, <https://doi.org/10.5194/acp-19-13827-2019>, 2019.

485 Meehl, G. A., and Arblaster, J. M.: GCM sensitivity experiments for the Indian monsoon and tropospheric biennial
486 oscillation transition conditions, J. Climate, 15, [https://doi.org/10.1175/1520-
487 0442\(2002\)015<0923:imgset>2.0.co;2](https://doi.org/10.1175/1520-0442(2002)015<0923:imgset>2.0.co;2), 2002.

488 Meehl, G.A., Shields, C., Arblaster, J.M., Annamalai, H., and Neale, R.: Intraseasonal, seasonal, and interannual
489 characteristics of regional monsoon simulations in CESM2, J. Adv. Model. Earth Sys., 12,
490 <https://doi.org/10.1029/2019MS001962>, 2020.

491 Meehl, G. A., Shields, C. A., Arblaster, J. M., Fasullo, J., Rosenbloom, N., Hu, A., et al.: Processes that contribute
492 to future South Asian monsoon differences in E3SMv2 and CESM2, Geophys. Res. Lett., 51,
493 <https://doi.org/10.1029/2024GL109056>, 2024.

494 Neale, R. B., Gettelman, A., Park, S., Chen, C.-C., Lauritzen, P. H., et al.: Description of the NCAR Community
495 Atmosphere Model (CAM 5.0), NCAR technical note, NCAR/TN-48, 274.
496 <https://doi.org/10.5065/D6N877R0>, 2012.

497 Persad, G., Samset, B.H., Wilcox, L.J., Allen, R.J., Bollasina, M.A., et al.: Rapidly evolving aerosol emissions are
498 a dangerous omission from near-term climate risk assessments, Environ. Res. Climate, 2,
499 <https://doi.org/10.1088/2752-5295/acd6af>, 2023.

500 Preethi, B., Mujumdar, M., Kripalani, R.H. et al.: Recent trends and tele-connections among South and East Asian
501 summer monsoons in a warming environment, Clim. Dynam., 48, [https://doi.org/10.1007/s00382-016-3218-
502 0](https://doi.org/10.1007/s00382-016-3218-0), 2017.

503 Rajesh, P. V., and Goswami, B. N.: Four-dimensional structure and sub-seasonal regulation of the Indian summer
504 monsoon multi-decadal mode, Clim. Dynam., 55, <https://doi.org/10.1007/s00382-020-05407-y>, 2020.

505 Rao, S.A., Dhakate, A.R., Saha, S.K. et al.: Why is Indian Ocean warming consistently?, Climatic Change, 110,
506 <https://doi.org/10.1007/s10584-011-0121-x>, 2012.

507 Rayner, N. A., Parker, D. E., Horton, E. B., Folland, C. K., Alexander, L. V., Rowell, D. P., Kent, E. C., and
508 Kaplan, A.: Global analyses of sea surface temperature, sea ice, and night marine air temperature since the late
509 nineteenth century, J. Geophys. Res., 108, <https://doi.org/10.1029/2002JD002670>, 2003.

510 Rodwell, M. J., and Hoskins, B. J.: Subtropical anticyclones and summer monsoons, J. Climate, 14,
511 [https://doi.org/10.1175/1520-0442\(2001\)014<3192:SAASM>2.0.CO;2](https://doi.org/10.1175/1520-0442(2001)014<3192:SAASM>2.0.CO;2), 2001.

512 Roxy, M. K., Ritika, K., Terray, P., and Masson, S.: The curious case of Indian Ocean warming. J. Climate, 27,

513 <https://doi.org/10.1175/JCLI-D-14-00471.1>, 2014.

514 Roxy, M., Ritika, K., Terray, P. et al.: Drying of Indian subcontinent by rapid Indian Ocean warming and a
515 weakening land-sea thermal gradient, *Nat. Commun.*, 6, <https://doi.org/10.1038/ncomms8423>, 2015.

516 Saha, A., and Ghosh, S.: Can the weakening of the Indian Monsoon be attributed to anthropogenic aerosols?
517 *Environ. Res. Commun.*, 1, <https://doi.org/10.1088/2515-7620/ab2c65>, 2019.

518 Salzmann, M., Weser, H., Cherian, R.: Robust response of Asian summer monsoon to anthropogenic aerosols in
519 CMIP5 models, *J. Geophys. Res. Atmos.*, 119, <https://doi.org/10.1002/2014JD021783>, 2014.

520 Salzmann, M., and Cherian, R.: On the enhancement of the Indian summer monsoon drying by Pacific
521 multidecadal variability during the latter half of the twentieth century, *J. Geophys. Res. Atmos.*, 120,
522 <https://doi.org/10.1002/2015JD023313>, 2015.

523 Samset, B. H., et al.: Climate impacts from a removal of anthropogenic aerosol emissions. *Geophys. Res. Lett.*,
524 45, <https://doi.org/10.1002/2017GL076079>, 2018.

525 Samset, B.H., Lund, M.T., Bollasina, M., et al.: Emerging Asian aerosol patterns. *Nat. Geosci.*, 12,
526 <https://doi.org/10.1038/s41561-019-0424-5>, 2019.

527 Schneider, U., Becker, A., Finger, P. et al.: GPCP's new land surface precipitation climatology based on quality-
528 controlled in situ data and its role in quantifying the global water cycle, *Theor. Appl. Climatol.*, 115,
529 <https://doi.org/10.1007/s00704-013-0860-x>, 2014,

530 Shao, Z., Wang, H., Geng, Y.F., et al.: East Asian summer monsoon response to anthropogenic aerosols
531 redistribution: contrasting 1950–1980 and 1980–2010 to understand the role of non-Asian forcing, *Clim.*
532 *Dynam.*, 62, <https://doi.org/10.1007/s00382-023-07016-x>, 2024.

533 Shawki, D., Voulgarakis, A., Chakraborty, A., Kasoar, M., and Srinivasan, J.: The South Asian monsoon response
534 to remote aerosols: Global and regional mechanisms, *J. Geophys. Res.*, 123,
535 <https://doi.org/10.1029/2018JD028623>, 2018.

536 Simpson, I. R., and Coauthors: The CESM2 single-forcing large ensemble and comparison to CESM1:
537 implications for experimental design. *J. Climate*, 36, <https://doi.org/10.1175/JCLI-D-22-0666.1>, 2023.

538 Smith, S. J., van Aardenne, J., Klimont, Z., Andres, R. J., Volke, A., and Delgado Arias, S.: Anthropogenic sulfur
539 dioxide emissions: 1850–2005, *Atmos. Chem. Phys.*, 11, <https://doi.org/10.5194/acp-11-1101-2011>, 2011.

540 Smith, D., Gillett, N. P., Simpson, I. R., Athanasiadis, P. J., Baehr, J., Bethke, I., et al.: Attribution of multi-annual
541 to decadal changes in the climate system: The large ensemble single forcing model intercomparison project

542 (LESMIP), *Front. Clim.*, 4, <https://doi.org/10.3389/fclim.2022.955414>, 2022.

543 Song, F., Zhou, T., and Qian, Y.: Responses of East Asian summer monsoon to natural and anthropogenic forcings
544 in the 17 latest CMIP5 models, *Geophys. Res. Lett.*, 41, <https://doi.org/10.1002/2013GL058705>, 2014.

545 Stier, P., van den Heever, S.C., Christensen, M.W., et al.: Multifaceted aerosol effects on precipitation, *Nat.*
546 *Geosci.*, 17, <https://doi.org/10.1038/s41561-024-01482-6>, 2024.

547 Swapna, P., Krishnan, R., and Wallace, J.M.: Indian Ocean and monsoon coupled interactions in a warming
548 environment, *Clim. Dynam.*, 42, <https://doi.org/10.1007/s00382-013-1787-8>, 2014.

549 Szopa, S., et al.: Short-Lived Climate Forcers. In *Climate Change 2021: The Physical Science Basis. Contribution*
550 *of Working Group I to the Sixth Assessment Report of the Intergovernmental Panel on Climate Change*
551 [Masson-Delmotte, V., P. Zhai, A. Pirani, S.L. Connors, C. Péan, S. Berger, N. Caud, Y. Chen, L. Goldfarb,
552 M.I. Gomis, M. Huang, K. Leitzell, E. Lonnoy, J.B.R. Matthews, T.K. Maycock, T. Waterfield, O. Yelekçi, R.
553 Yu, and B. Zhou (eds.)]. Cambridge University Press, Cambridge, United Kingdom and New York, NY, USA,
554 pp. 817–922, <https://doi.org/10.1017/9781009157896.008>, 2021.

555 Takaya, K., and Nakamura, H.: A formulation of a phase-independent wave-activity flux for stationary and
556 migratory quasigeostrophic eddies on a zonally varying basic flow, *J. Atmos. Sci.*, 58,
557 [https://doi.org/10.1175/1520-0469\(2001\)058<0608:AFOAPI>2.0.CO;2](https://doi.org/10.1175/1520-0469(2001)058<0608:AFOAPI>2.0.CO;2), 2001.

558 Turner, A., and Annamalai, H.: Climate change and the South Asian summer monsoon, *Nature Clim. Change* 2,
559 <https://doi.org/10.1038/nclimate1495>, 2012

560 Undorf, S., Bollasina, M., Booth, B., and Hegerl, G.: Contrasting the effects of the 1850-1975 increase in sulphate
561 aerosols from North America and Europe on the Atlantic in the CESM, *Geophys. Res. Lett.*, 45,
562 <https://doi.org/10.1029/2018GL079970>, 2018.

563 Undorf, S., Polson, D., Bollasina, M. A., Ming, Y., Schurer, A., and Hegerl, G. C.: Detectable impact of local and
564 remote anthropogenic aerosols on the 20th century changes of West African and South Asian monsoon
565 precipitation, *J. Geophys. Res.*, 123, <https://doi.org/10.1029/2017JD027711>, 2018.

566 Wang, Q., Wang, Z., and Zhang, H.: Impact of anthropogenic aerosols from global, East Asian, and non-East
567 Asian sources on East Asian summer monsoon system, *Atmos. Res.*, 183,
568 <https://doi.org/10.1016/j.atmosres.2016.08.023>, 2017.

569 Wang, B., and Coauthors: Toward predicting changes in the land monsoon rainfall a decade in advance. *J. Climate*,
570 31, <https://doi.org/10.1175/JCLI-D-17-0521.1>, 2018.

571 Wang, Z., Mu, J., Yang, M., and Yu, X.: Reexamining the mechanisms of East Asian summer monsoon changes
572 in response to non–East Asian anthropogenic aerosol forcing. *J. Climate*, 33, [https://doi.org/10.1175/JCLI-D-](https://doi.org/10.1175/JCLI-D-19-0550.1)
573 [19-0550.1](https://doi.org/10.1175/JCLI-D-19-0550.1), 2020.

574 Wang, Z., Lin, L., Xu, Y., et al.: Incorrect Asian aerosols affecting the attribution and projection of regional climate
575 change in CMIP6 models, *npj Clim. Atmos. Sci.*, 4, <https://doi.org/10.1038/s41612-020-00159-2>, 2021.

576 Wang, Z., Feng, J., Diao, C., Li, Y., Lin, L., and Xu, Y.: Reduction in European anthropogenic aerosols and the
577 weather conditions conducive to PM_{2.5} pollution in North China: a potential global teleconnection pathway,
578 *Environ. Res. Lett.*, 16, <https://doi.org/10.1088/1748-9326/ac269d>, 2021.

579 Watanabe, M.: Asian jet waveguide and a downstream extension of the North Atlantic Oscillation, *J. Climate*, 17,
580 <https://doi.org/10.1175/JCLI-3228.1>, 2004.

581 Westervelt, D. M., Conley, A. J., Fiore, A. M., Lamarque, J.-F., Shindell, D. T., Previdi, M., Mascioli, N. R.,
582 Faluvegi, G., Correa, G., and Horowitz, L. W.: Connecting regional aerosol emissions reductions to local and
583 remote precipitation responses, *Atmos. Chem. Phys.*, 18, 12461–12475, [https://doi.org/10.5194/acp-18-](https://doi.org/10.5194/acp-18-12461-2018)
584 [12461-2018](https://doi.org/10.5194/acp-18-12461-2018), 2018.

585 Wilcox, L. J., Allen, R. J., Samset, B. H., Bollasina, M. A., et al.: The Regional Aerosol Model Intercomparison
586 Project (RAMIP), *Geosci. Model Dev.*, 16, <https://doi.org/10.5194/gmd-16-4451-2023>, 2023.

587 Wilcox L. J., Liu, Z., Samset, B. H., et al.: Accelerated increases in global and Asian summer monsoon
588 precipitation from future aerosol reductions, *Atmos. Chem. Phys.*, 20, [https://doi.org/10.5194/acp-20-11955-](https://doi.org/10.5194/acp-20-11955-2020)
589 [2020](https://doi.org/10.5194/acp-20-11955-2020), 2020.

590 Willmott, C. J., and Matsuura, K.: Smart interpolation of annually averaged air temperature in the United States,
591 *J. Appl. Meteor. Climatol.*, 34, [https://doi.org/10.1175/1520-0450\(1995\)034<2577:SIOAAA>2.0.CO;2](https://doi.org/10.1175/1520-0450(1995)034<2577:SIOAAA>2.0.CO;2),
592 1995.

593 Wu, G. X., Li, Z. Q., Fu, C. B., Zhang, X. Y., Zhang, R. Y., Zhang, R. H., et al.: Advances in studying interactions
594 between aerosols and monsoon in China. *Science China Earth Sciences*, 59, [https://doi.org/10.1007/s11430-](https://doi.org/10.1007/s11430-015-5198-z)
595 [015-5198-z](https://doi.org/10.1007/s11430-015-5198-z), 2016.

596 Xiang, B., Xie, S. P., Kang, S. M. et al.: An emerging Asian aerosol dipole pattern reshapes the Asian summer
597 monsoon and exacerbates northern hemisphere warming, *npj Clim. Atmos. Sci.*, 6,
598 <https://doi.org/10.1038/s41612-023-00400-8>, 2023.

599 Xie, P., and Arkin, P. A.: Global precipitation: A 17-Year monthly analysis based on gauge observations, satellite

600 estimates, and numerical model outputs, *Bull. Amer. Meteor. Soc.*, 78, [https://doi.org/10.1175/1520-](https://doi.org/10.1175/1520-0477(1997)078<2539:GPAYMA>2.0.CO;2)
601 [0477\(1997\)078<2539:GPAYMA>2.0.CO;2](https://doi.org/10.1175/1520-0477(1997)078<2539:GPAYMA>2.0.CO;2), 1997.

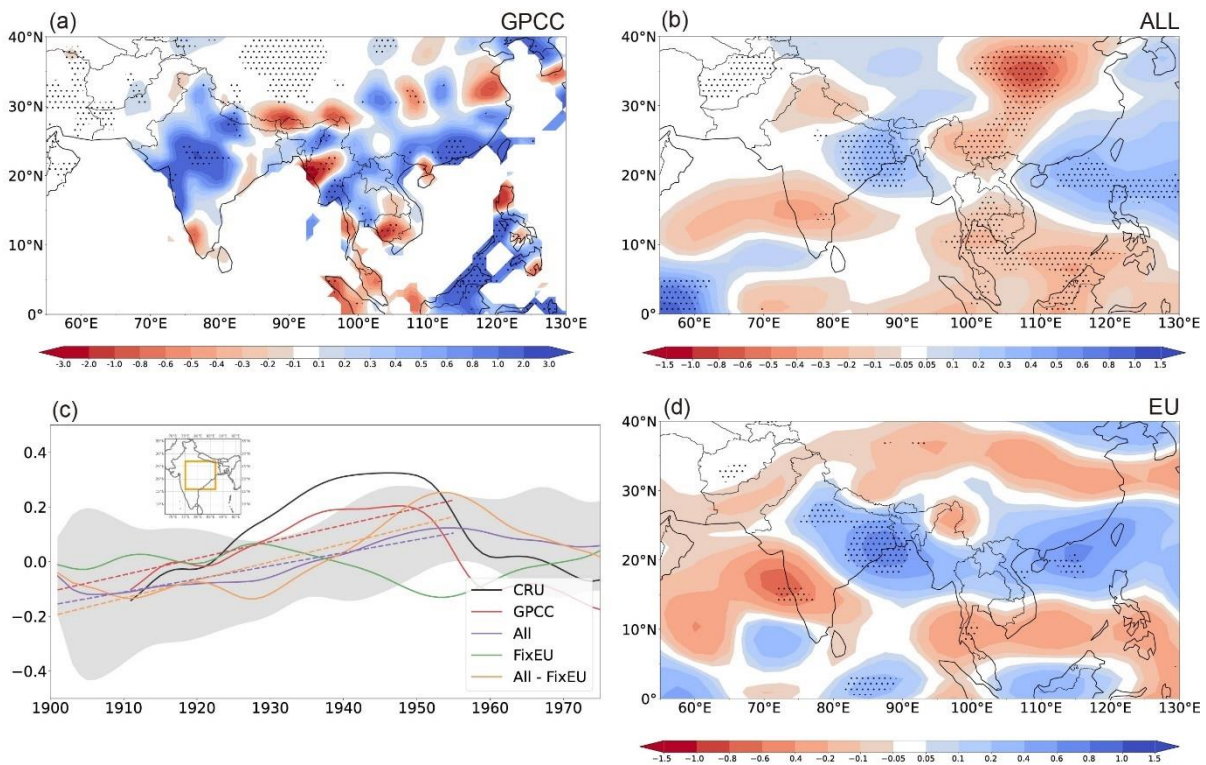
602 Zelinka, M. D., Andrews, T., Forster, P. M., and Taylor, K. E.: Quantifying components of aerosol-cloud-radiation
603 interactions in climate models, *J. Geophys. Res. Atmos.*, 119, [https://doi:10.1002/2014JD021710](https://doi.org/10.1002/2014JD021710), 2014.

604 Zelinka, M. D., Smith, C. J., Qin, Y., and Taylor, K. E.: Comparison of methods to estimate aerosol effective
605 radiative forcings in climate models, *Atmos. Chem. Phys.*, 23, <https://doi.org/10.5194/acp-23-8879-2023>,
606 2023.

607 Zhang, L., and Zhou, T.: An assessment of monsoon precipitation changes during 1901–2001. *Clim. Dynam.*, 37,
608 <https://doi.org/10.1007/s00382-011-0993-5>, 2011.

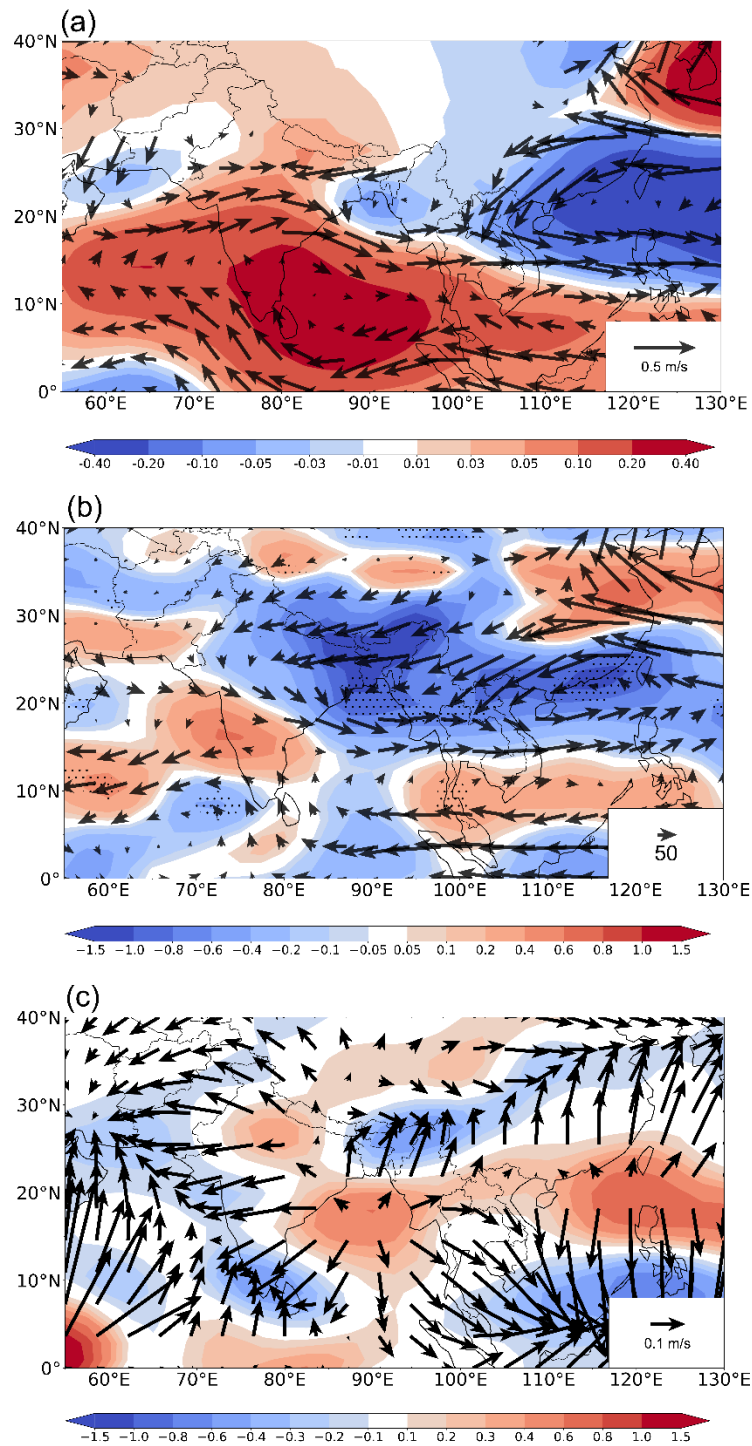
609

610 **Figures**
611



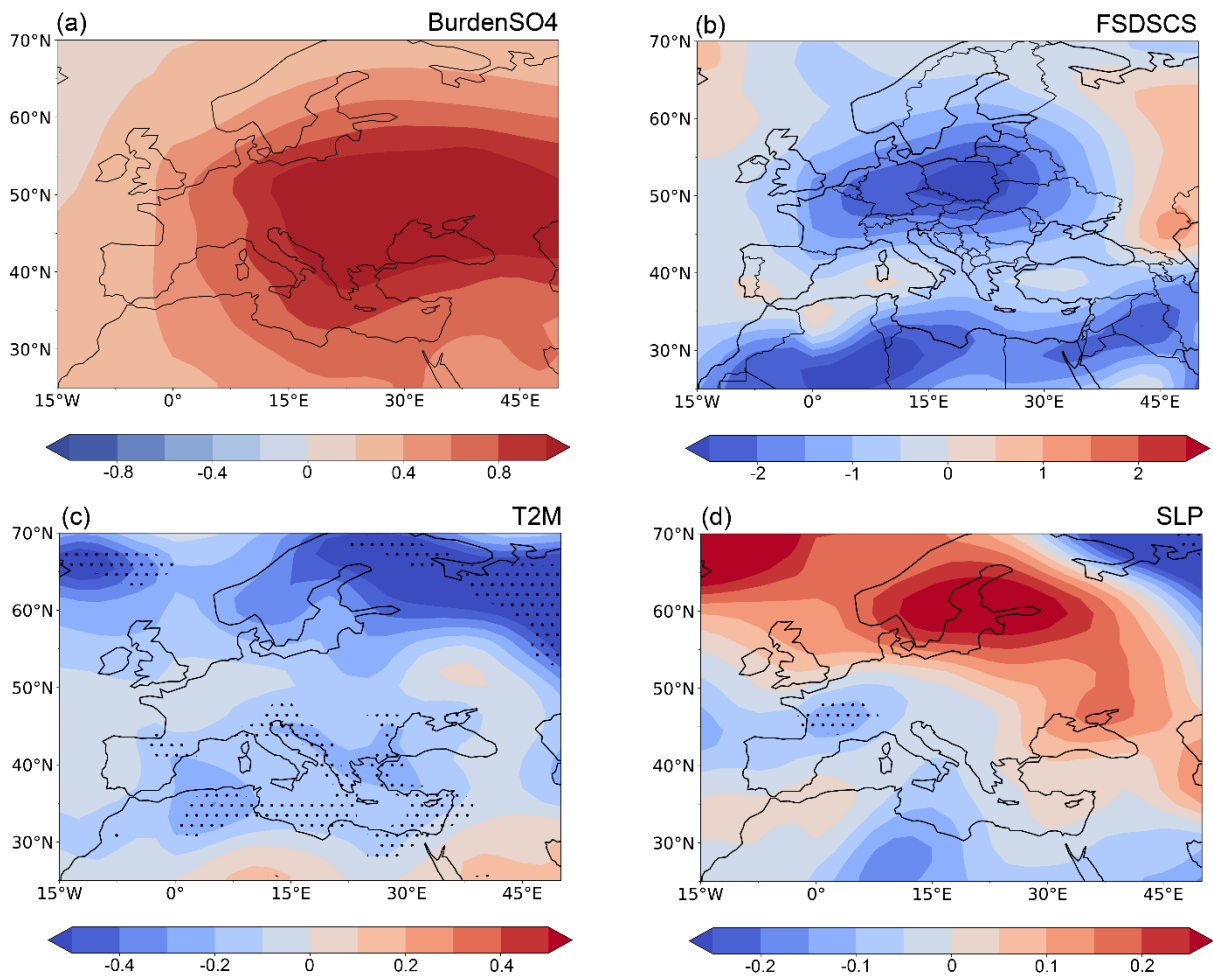
612
613
614
615
616
617
618
619
620
621
622
623
624
625
626
627
628

Figure 1. (a)-(b): Spatial patterns of the 1901-1955 linear trends of JJA precipitation ($\text{mm day}^{-1} (55 \text{ years})^{-1}$) for (a) GPCC, (b) the all-forcing ensemble (ALL), and (d) the difference between ALL and the all-forcing experiment with fixed preindustrial aerosol emissions over Europe (fixEU), representing the impact of EU aerosols. The black dots mark the grid points for which the trend exceeds the 90% significance level according to the two-tailed Student's t-test. (c): Time series of area-averaged JJA precipitation anomalies (mm day^{-1} ; deviations from the 1901-2000 climatology) over central-northern India (land-only points within 75° – 87°E , 16° – 27°N ; area shown in inset map) smoothed with 11-year running means to highlight low-frequency (multi-decadal) fluctuations. The black and red lines represent observations (CRU and GPCC, respectively), while the purple, green and orange lines represent the ensemble means of ALL, fixEU, and their difference (EU). The grey shading represents the standard deviation of the eight-member ALL ensemble around the mean. The 1901-1955 least-squares linear trends of the simulated time series are shown as dashed lines in the corresponding colours. Note that the interval for the simulated changes is half of that used for the observations.



629

630 **Figure 2.** Spatial patterns of the 1901-1955 linear trends of the JJA average (a) 850-hPa winds ($\text{m s}^{-1} (55 \text{ years})^{-1}$) and 925-hPa streamfunction (colors, $10^6 \text{ m}^2 \text{ s}^{-1} (55 \text{ years})^{-1}$), (b) 1000-300 hPa vertically integrated moisture
 631 transport (vectors, $\text{Kg m}^{-1} \text{ s}^{-1}$) and its divergence (shades, $\text{mm d}^{-1} (55 \text{ years})^{-1}$), (c) 150-hPa divergent circulation
 632 ($\text{m s}^{-1} (55 \text{ years})^{-1}$) and its divergence (shades; $10^{-6} \text{ s}^{-1} (55 \text{ years})^{-1}$) associated with increased European sulphate
 633 aerosols (difference between the ALL and fixEU ensemble means). The black dots in (b) mark the grid points for
 634 which the trend exceeds the 90% significance level according to the two-tailed Student's t-test.
 635



637

638

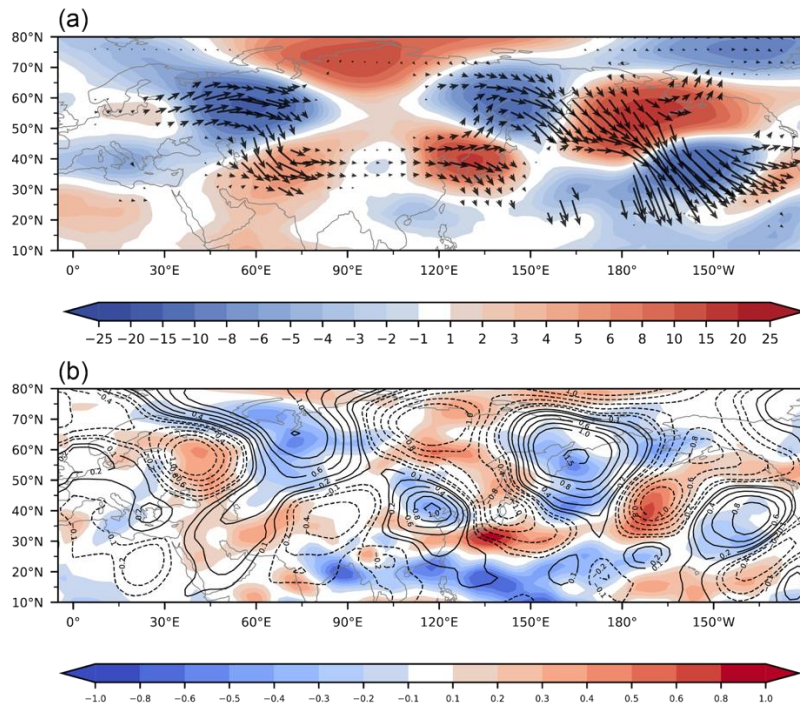
639 **Figure 3.** Spatial patterns of the 1901-1955 linear trends of the JJA average (a) column sulphate aerosol burden640 ($10^{-5} \text{ kg m}^{-2} (55 \text{ years})^{-1}$), (b) surface clear-sky downward shortwave radiation ($\text{W m}^{-2} (55 \text{ years})^{-1}$), (c) 2-m air641 temperature ($\text{K} (55 \text{ years})^{-1}$), and (d) sea level pressure ($\text{hPa} (55 \text{ years})^{-1}$) associated with increased European

642 sulphate aerosols (difference between the ALL and fixEU ensemble means). The black dots in (c) and (d) mark

643 the grid points for which the trend exceeds the 90% significance level according to the two-tailed Student's t-test.

644

645



646

647

648 **Figure 4.** Spatial patterns of the 1901-1955 linear trends of the JJA average (a) 300-hPa wave activity flux
649 (vectors; $10^{-4} \text{ m}^2 \text{ s}^{-2} (55 \text{ years})^{-1}$) and streamfunction (shades; $10^5 \text{ m}^2 \text{ s}^{-1} (55 \text{ years})^{-1}$), and (b) 300-hPa meridional
650 wind (contours; $\text{m s}^{-1} (55 \text{ years})^{-1}$) and 500-hPa vertical velocity (shades; $10^{-2} \text{ Pa s}^{-1} (55 \text{ years})^{-1}$) associated with
651 increased European sulphate aerosols (difference between the ALL and fixEU ensemble means).